

# Modelling and Simulation of Flow and Heat Transfer of Ferrofluid under Magnetic Field of Neodymium Block Magnet



S. Morteza Mousavi<sup>a</sup>, A. Ali Rabienataj Darzi<sup>b,\*</sup>, Ming Li<sup>c</sup>

<sup>a</sup> Faculty of Mechanical Engineering, Babol Noshirvani University of Technology, Babol, Iran

<sup>b</sup> Department of Mechanical Engineering, University of Mazandaran, Babolsar, Iran

<sup>c</sup> School of Engineering, Macquarie University, Sydney, NSW 2109, Australia

## ARTICLE INFO

### Article history:

Received 12 May 2021

Revised 7 October 2021

Accepted 10 October 2021

Available online 20 October 2021

### Keywords:

Convection

Ferrofluid

FHD

MHD

Permanent magnet

## ABSTRACT

Neodymium magnets are the strongest type of permanent magnet commercially available. This investigation aims to numerically study the behavior of ferrofluids in the presence of neodymium block magnets which could be used in a wide range of applications. The problem formulation is derived using the principles of ferrohydrodynamics (FHD) and magnetohydrodynamics (MHD), and the finite volume method is employed for solving the equations. The flow of water- $\text{Fe}_3\text{O}_4$  magnetic nanofluid at  $250 \leq \text{Re} \leq 2300$  in a three-dimensional channel under heat flux exposed to a block neodymium magnet is considered. The results indicate that the magnet can significantly affect the flow field and heat transfer while FHD effects are completely dominant and MHD effects are ignorable. In the presence of the magnet, a secondary flow is created, which is more significant for low Reynolds numbers. Applying the magnetic field increases the heat transfer so that at  $\text{Re}=250$ , where the heat transfer is low, it can increase the Nusselt number by a factor of 2. Moreover, the magnetic field substantially increases the wall skin friction. Considering both the increments of heat transfer and friction, the Reynolds number of 1500 has the maximum thermal performance factor. With increasing Reynolds number or distance between the magnet and channel, the magnetic effect decreases. It is found that the thermal performance factor is increased by reducing the distance of the magnet and channel. In addition, if the height of the magnet is decreased by half (from 1 cm to 0.5 cm), the thermal performance factor improves by 6%.

© 2021 Elsevier Inc. All rights reserved.

## 1. Introduction

The improvement of fluids' thermophysical properties by the addition and dispersion of nanometer-sized metal particles with much higher thermal conductivity than the liquids' is an effective way to enhance the heat transfer rate. Nanofluids were first introduced by Choi and Eastman [1] and since then have been studied in various applications. The behavior of nanofluids under the influence of magnetic fields has been investigated by many researchers. A magnetic field can affect the fluid dynamics and heat transfer [2–8]. Nanofluid flows affected by the magnetic fields have been simulated based on the principles of Ferrohydrodynamics (FHD) [9] and Magnetohydrodynamics (MHD) [10], taking into account the gradients of magnetic fields, magnetization and electrical conductivity of the nanofluids.

\* Corresponding author.

E-mail addresses: [smorteza\\_mousavi@yahoo.com](mailto:smorteza_mousavi@yahoo.com) (S.M. Mousavi), [a.rabienataj@umz.ac.ir](mailto:a.rabienataj@umz.ac.ir) (A.A.R. Darzi), [ming.li@mq.edu.au](mailto:ming.li@mq.edu.au) (M. Li).

## Nomenclature

### Symbols

$2a$	width of the magnet (m)
$2b$	length of the magnet (m)
$B$	magnetic field induction (T)
$B_r$	residual magnetism (T)
$c$	height of the magnet (m)
$C$	pressure gradient parameter $((dp/dy)/\mu)$ ( $1 \text{ m}^{-1} \text{ s}^{-1}$ )
$C_f$	skin-friction coefficient $(\tau_w/1/2 \rho_{nf} V_0^2)$
$c_p$	specific heat at constant pressure ( $\text{J kg}^{-1} \text{ K}^{-1}$ )
$d$	particle diameter (m)
$D$	distance between the channel and magnet (m)
$g$	gravitational acceleration ( $\text{m s}^{-2}$ )
$h$	height of the channel (m)
$h_c$	heat transfer coefficient ( $\text{W m}^{-2} \text{ K}^{-1}$ )
$H$	magnetic field intensity ( $\text{A m}^{-1}$ )
$H_x$	magnetic field intensity component along the x direction ( $\text{A m}^{-1}$ )
$H_y$	magnetic field intensity component along the y direction ( $\text{A m}^{-1}$ )
$H_z$	magnetic field intensity component along the z direction ( $\text{A m}^{-1}$ )
$J$	electric current density ( $\nabla \times \mathbf{H} = \mathbf{J} = \sigma_{nf}(\mathbf{V} \times \mathbf{B})$ ) ( $\text{A m}^{-2}$ )
$k$	thermal conductivity ( $\text{W m}^{-1} \text{ K}^{-1}$ )
$k_B$	Boltzmann constant $= 1.3806503 \times 10^{-23}$ ( $\text{J K}^{-1}$ )
$L$	Langevin function
$m$	particle magnetic moment ( $\text{Am}^2$ )
$M$	magnetization ( $\text{A m}^{-1}$ )
$M_s$	saturation magnetization ( $\text{A m}^{-1}$ )
$Nu$	Nusselt number $(h_c h/k_{nf} = q'' h/k_{nf} (T_{wall} - T_0))$
$P$	pressure (Pa)
$q''$	heat flux ( $\text{W m}^{-2}$ )
$Re$	Reynolds number $(\rho_{nf} V_0 h / \mu_{nf})$
$T$	temperature (K)
$T_0$	inlet flow temperature (K)
$V=(u,v,w)$	velocity field ( $\text{m s}^{-1}$ )
$V_0$	inlet velocity ( $\text{m s}^{-1}$ )
$x$	x-Cartesian coordinate (m)
$y$	y-Cartesian coordinate (m)
$z$	z-Cartesian coordinate (m)

### Greek Letters

$\beta$	thermal expansion coefficient ( $\text{K}^{-1}$ )
$\mu$	dynamic viscosity ( $\text{kg m}^{-1} \text{ s}^{-1}$ )
$\mu_0$	magnetic permeability of vacuum $= 4\pi \times 10^{-7}$ ( $\text{T m A}^{-1}$ )
$\mu_B$	Bohr magneton $= 9.27 \times 10^{-24}$ ( $\text{Am}^2$ )
$\xi$	Langevin parameter
$\rho$	density ( $\text{kg m}^{-3}$ )
$\sigma$	electrical conductivity ( $\text{s m}^{-1}$ )
$\tau_w$	wall shear stress (Pa)
$\phi$	particle volume fraction
$\Phi$	viscous dissipation function

### Subscripts

$av$	average
$f$	base fluid
$l$	local
$nf$	nanofluid
$p$	particle

A magnetic fluid is a colloidal solution including magnetic particles suspended in a carrier fluid. For the dispersion of the particles in the carrier fluid and avoiding agglomeration or particle settling, a surfactant or coatings is used. The most common magnetic fluids are ferrofluids and paramagnetic solutions [11].

In ferrofluids, the diameter of particles can vary between 10 and 50 nanometers, and these particles are usually made out of magnetite or ferrite [11]. The particles must not be too small because at sizes less than 1 or 2 nanometers, their magnetic properties tend to disappear [12]. A ferrofluid consists of 1 to 5 percent magnetic particles by volume and 10 percent surfactant, and the remainder is the carrier fluid. In the absence of magnetic fields, the magnetic moments of the particles align randomly, similar to a paramagnetic material, and the net magnetization of the solution is equal to zero. In the presence of a magnetic field, magnetic particles in a ferrofluid are instantly magnetized. This means that the magnetic moments of the particles are immediately aligned with the magnetic field lines. The magnetic forces holding a ferrofluid in place are proportional to the magnetization of the magnetic particles and the applied magnetic field. In the presence of a weak magnetic field, the thermal energy from the agitation of the solution overcomes the magnetic forces holding the ferrofluid in place, and the particles randomly disperse [11].

Many experimental and numerical studies have been carried out on ferrofluid flows exposed to magnetic fields. Ganguly *et al.* [13] investigated the heat transfer of a ferrofluid in a cavity with a temperature difference between its two walls in the presence of a non-uniform magnetic field. The results show that convective heat transfer occurs due to the temperature gradients and magnetic force, and with increase of the temperature difference and magnetic field strength, the heat transfer increases. Li and Xuan [14] studied the convective heat transfer of water- $\text{Fe}_3\text{O}_4$  magnetic fluid flowing over a heated wire in a channel in the presence of a uniform magnetic field and a magnetic field gradient. They observed that applying a magnetic field gradient along with the main flow direction is significantly effective in the enhancement of the heat transfer. In addition, they found that the concentration of magnetic nanoparticles around the heated wire, which may decrease or increase under the influence of the magnetic force, plays a major role in the heat transfer between the wire and the magnetic fluid. Aminfar *et al.* [15] employed the mixture model to numerically investigate the effects of a linearly-varying magnetic field on a kerosene- $\text{Fe}_3\text{O}_4$  magnetic fluid in a vertical tube under uniform heat flux. They found that by applying the magnetic field, the heat transfer can be controlled, either increased or decreased. The influence of a magnetic field varying linearly perpendicular to the main flow direction on the fluid dynamics and heat transfer of water- $\text{Fe}_3\text{O}_4$  magnetic fluid flow in a curved tube was numerically studied by Aminfar *et al.* [16]. Their results revealed that the secondary flow augmentation caused by centrifugal and magnetic forces increases the heat transfer rate. Wang *et al.* [17] conducted an experimental study on the viscosity of water- $\text{Fe}_3\text{O}_4$  magnetic fluid exposed to a magnetic field of 0 to 30 mT. They observed that the viscosity of the nanofluid increases with increase of the magnetic strength and nanofluid volume fraction, and decreases with increase of the temperature. Based on the experimental results, they presented a correlation for the viscosity of water- $\text{Fe}_3\text{O}_4$  nanofluid which is a function of the magnetic induction, nanofluid volume fraction and temperature. Mousavi *et al.* [18] numerically investigated the fluid dynamics and heat transfer of water- $\text{Fe}_3\text{O}_4$  magnetic fluid in a helical tube in the presence of a non-uniform magnetic field. Their results show that applying the magnetic field can significantly increase the heat transfer and wall shear stress, and a magnetic gradient in which the thermal-hydraulic performance is optimum, can be found.

Cheng and Li [19] experimentally studied the natural convection heat transfer in diester- $\text{Fe}_3\text{O}_4$  ferrofluid exposed to the magnetic field of a block permanent NdFeB (neodymium iron boron) magnet between two heated and cooled plates. Their results indicate that the heat transfer is enhanced in the presence of the magnet. The heat transfer of water- $\text{Fe}_3\text{O}_4$  magnetic fluid in a laminar flow regime ( $\text{Re} < 830$ ) in the presence of NdFeB, grade 42 block permanent magnets was experimentally studied by Azizian *et al.* [20]. The results show that the heat transfer of the magnetite nanofluid can be increased up to 300% by applying the magnetic field. Wang *et al.* [21] experimentally studied the effects of ring permanent magnets (NdFeB N42) on laminar convective heat transfer of water- $\text{Fe}_3\text{O}_4$  magnetic fluid in a pipe. A pair of magnets was encapsulated into one plastic cannula and the cannula was added over the pipe. The distance between the surfaces of the pipe and magnet is 16.5 mm. Their results show that in the presence of a cannula, the heat transfer is enhanced by 26.5% and 54.5% at  $\text{Re} = 391$  and 805, respectively. Valitabar *et al.* [22] experimentally investigated the forced convection heat transfer of water- $\text{Fe}_3\text{O}_4$  magnetic fluid in a channel under five block permanent Neodymium magnets. The heat transfer characteristics at the different magnet distances from the test section, in the range from 2 mm to 80 mm, were compared and it is revealed that the maximum heat transfer is achieved at the minimum distance of magnets from the channel (2 mm). Tetuko *et al.* [23] conducted experiments on the heat transfer of water- $\text{Fe}_3\text{O}_4$  magnetic fluid in a pipe in laminar flows ( $\text{Re} = 171, 228$  and 285) under the influence of the magnetic field of a pair of half circular permanent magnets (NdFeB) attached to the pipe. The experimental results indicate that the magnetic field increases the convection heat transfer. The heat transfer and flow characteristics of the laminar flow of water- $\text{Fe}_3\text{O}_4$  magnetic fluid affected by different configurations of block permanent NdFeB (N40) magnets in a tube were experimentally investigated by Sun *et al.* [24]. The results show that applying the magnetic field enhances the heat transfer so that at  $\text{Re} = 1080$ , the heat transfer rose up to 32.0%. Moreover, the magnetic field increases the pressure drop, but this effect is weaker than the heat transfer enhancement effect.

Since neodymium magnets are known as the strongest type of permanent magnet commercially available [25], the simulation of ferrofluid flows in the presence of this kind of magnet can be useful and practical. As well as in cooling and heating devices [26–30], this type of magnet could be applicable in medical engineering in applications such as magnetic cell separation [31–34], magnetic drug targeting [35–37], magnetic hyperthermia [38–41] and magnetic wound healing [42, 43]. In this study, the fluid dynamics and heat transfer of water- $\text{Fe}_3\text{O}_4$  magnetic fluid exposed to a block neodymium magnet is investigated. The impacts of the distance between the channel and block magnet and the height of the magnet are

**Table 1**  
Physical properties of the nanofluid components [47].

	$\rho$ (kg m <sup>-3</sup> )	$c_p$ (J kg <sup>-1</sup> K <sup>-1</sup> )	$k$ (W m <sup>-1</sup> K <sup>-1</sup> )	$\beta$ (K <sup>-1</sup> )	$\sigma$ (s m <sup>-1</sup> )	$\mu$ (kg m <sup>-1</sup> s <sup>-1</sup> )
<b>Water</b>	998.2	4182	0.6	0.00021	0.05	0.001003
<b>Fe<sub>3</sub>O<sub>4</sub></b>	5200	670	6	0.000013	25000	-

studied. In addition, the average magnitude of FHD and MHD components are separately compared to analyze the influence of the magnetic terms.

## 2. Theoretical formulation

### 2.1. Problem statement and governing equations

The three-dimensional, steady, laminar flow of an incompressible and Newtonian water-Fe<sub>3</sub>O<sub>4</sub> nanofluid in a channel in the presence of the magnetic field of a block permanent magnet is considered. The geometry of the channel is schematically shown in Fig. 1: the cross-section of the channel is a square with the sides of  $h=0.01$  m, and the length of the channel equals  $28h$ . Moreover, the top wall of the middle section of the channel with a length of  $8h$  is heated with a constant and uniform heat flux of  $q''=25000$  W/m<sup>2</sup>.

A NdFeB magnet of 1.3 T residual magnetism with the dimensions of  $0.01$  m  $\times$   $0.04$  m  $\times$   $0.01$  m (width  $\times$  length  $\times$  height) is placed under the channel at the distance of  $D$ , as in the schematic model shown in Fig. 1. The magnetic field intensity components along the  $x$ ,  $y$  and  $z$  directions presented by McCaig and Clegg [44] are as given in Eqs. (1) to (3) [45], for which the local coordinate system for the equations and the poles of the magnet are shown in Fig. 1,

$$H_x = \frac{B_r}{4\pi\mu_0} \log_e \left\{ \frac{(y+b)+[(y+b)^2+(x-a)^2+z^2]^{1/2}}{(y-b)+[(y-b)^2+(x-a)^2+z^2]^{1/2}} \times \frac{(y-b)+[(y-b)^2+(x+a)^2+z^2]^{1/2}}{(y-b)+[(y-b)^2+(x+a)^2+z^2]^{1/2}} \right\} - \frac{B_r}{4\pi\mu_0} \log_e \left\{ \frac{(y+b)+[(y+b)^2+(x-a)^2+(z+c)^2]^{1/2}}{(y-b)+[(y-b)^2+(x-a)^2+(z+c)^2]^{1/2}} \times \frac{(y-b)+[(y-b)^2+(x+a)^2+(z+c)^2]^{1/2}}{(y+b)+[(y+b)^2+(x+a)^2+(z+c)^2]^{1/2}} \right\} \quad (1)$$

$$H_y = \frac{B_r}{4\pi\mu_0} \log_e \left\{ \frac{(x+a)+[(y-b)^2+(x+a)^2+z^2]^{1/2}}{(x-a)+[(y-b)^2+(x-a)^2+z^2]^{1/2}} \times \frac{(x-a)+[(y-b)^2+(x-a)^2+z^2]^{1/2}}{(x-a)+[(y-b)^2+(x-a)^2+z^2]^{1/2}} \right\} - \frac{B_r}{4\pi\mu_0} \log_e \left\{ \frac{(x+a)+[(y-b)^2+(x+a)^2+(z+c)^2]^{1/2}}{(x-a)+[(y-b)^2+(x-a)^2+(z+c)^2]^{1/2}} \times \frac{(x-a)+[(y-b)^2+(x-a)^2+(z+c)^2]^{1/2}}{(x+a)+[(y-b)^2+(x-a)^2+(z+c)^2]^{1/2}} \right\} \quad (2)$$

$$H_z = \frac{B_r}{4\pi\mu_0} \left\{ \tan^{-1} \left[ \frac{(x+a)(y+b)}{z[(x+a)^2+(y+b)^2+z^2]^{1/2}} \right] + \tan^{-1} \left[ \frac{(x-a)(y-b)}{z[(x-a)^2+(y-b)^2+z^2]^{1/2}} \right] - \tan^{-1} \left[ \frac{(x+a)(y-b)}{z[(x+a)^2+(y-b)^2+z^2]^{1/2}} \right] - \tan^{-1} \left[ \frac{(x-a)(y+b)}{z[(x-a)^2+(y+b)^2+z^2]^{1/2}} \right] \right\} - \frac{B_r}{4\pi\mu_0} \left\{ \tan^{-1} \left[ \frac{(x+a)(y+b)}{(z+c)[(x+a)^2+(y+b)^2+(z+c)^2]^{1/2}} \right] + \tan^{-1} \left[ \frac{(x-a)(y-b)}{(z+c)[(x-a)^2+(y-b)^2+(z+c)^2]^{1/2}} \right] - \tan^{-1} \left[ \frac{(x+a)(y-b)}{(z+c)[(x+a)^2+(y-b)^2+(z+c)^2]^{1/2}} \right] - \tan^{-1} \left[ \frac{(x-a)(y+b)}{(z+c)[(x-a)^2+(y+b)^2+(z+c)^2]^{1/2}} \right] \right\} \quad (3)$$

The magnitude of the magnetic field intensity is given by Eq. (4), and its distribution on a cross-section for  $2a=0.1$ ,  $2b=0.04$ ,  $c=0.01$  and  $Br=1.3$  is shown in Fig. 1.

$$H = \sqrt{H_x^2 + H_y^2 + H_z^2} \quad (4)$$

Hydrodynamically fully developed flow with average axial velocity  $V_0$  with the distribution presented in Eq. (5) [46], and temperature  $T_0=300$  K enters the channel.

$$\nu(x, z) = -\frac{16C(h/2)^2}{\pi^3} \sum_{n=1,3,\dots}^{\infty} \frac{1}{n^3} (-1)^{(n-1)/2} \left[ 1 - \frac{\cosh(\frac{n\pi(z-(h/2)+D)}{h})}{\cosh(\frac{n\pi h/2}{h})} \right] \cos\left(\frac{n\pi x}{h}\right) \quad (5)$$

$$C = -\frac{3V_0}{(h/2)^2} \left[ \frac{1}{1 - \frac{192}{\pi^5} \sum_{n=1,3,\dots}^{\infty} \frac{1}{n^5} \tanh(\frac{n\pi h/2}{h})} \right]$$

On all walls, the no-slip condition is applied, and at the channel outlet, the diffusion fluxes normal to the outlet plane are considered zero for all of the flow parameters.

The water-based nanofluid consists of a 4% volume fraction of spherical shape Fe<sub>3</sub>O<sub>4</sub> particles with the mean diameter of 10 nm. The physical properties of the base fluid and particles are given in Table 1 [47]. The properties of the nanofluid are presumed to be constant with the exception of the density in the buoyancy force, which is based on the Boussinesq

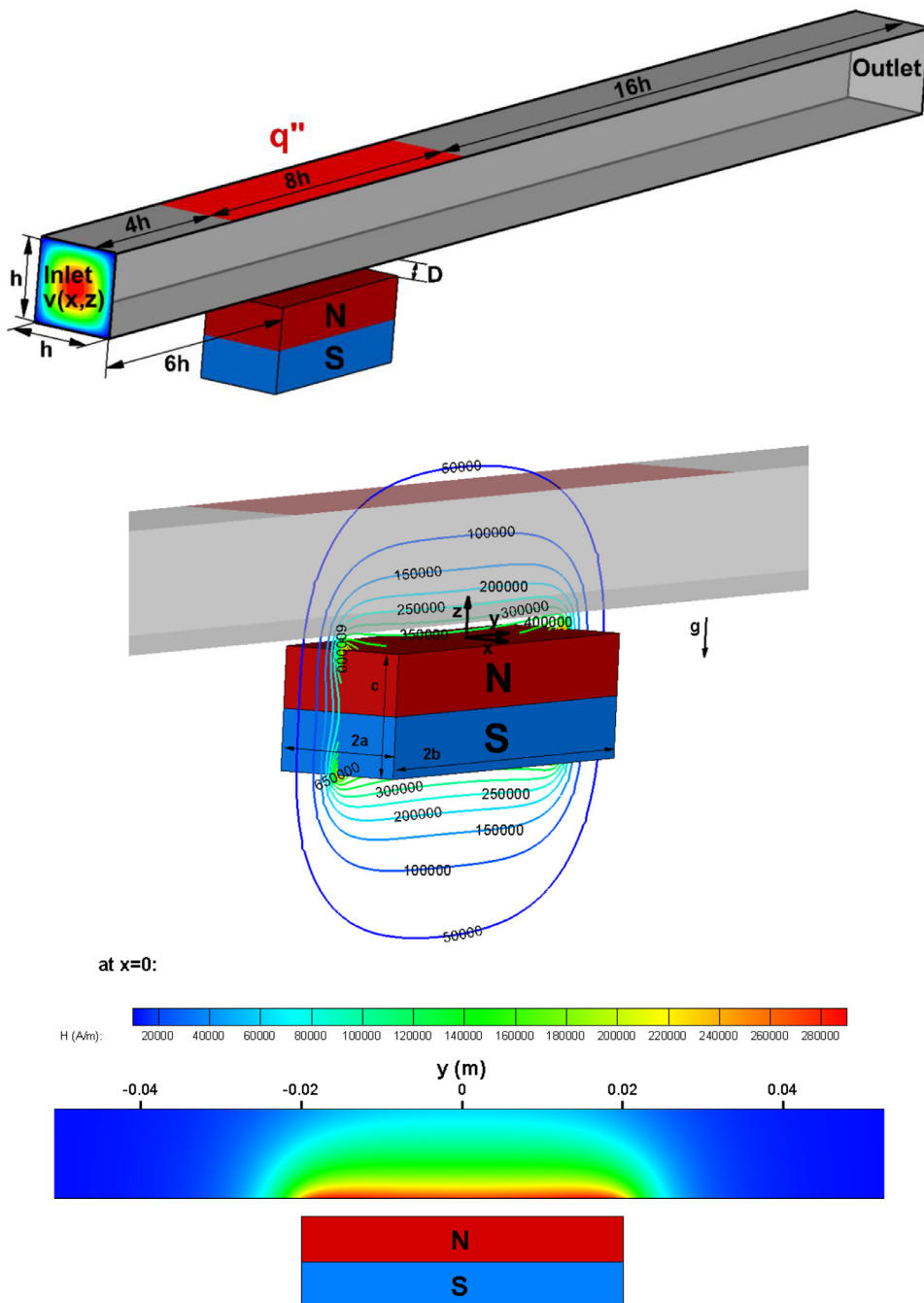


Fig. 1. Geometry of problem.

approximation. It is supposed that the nanoparticles are well dispersed in the base fluid and therefore, the nanofluid is assumed homogeneous. In addition, it is considered that the slip velocity of the continuous phase and nanoparticles is negligible, and there is a thermal equilibrium between them. Based on these assumptions, the nanofluid can be treated as a single-phase fluid with the properties calculated according to the concentrations of water and  $\text{Fe}_3\text{O}_4$ .

The changes of viscosity in the presence of the magnetic field are ignored.  $\mathbf{H}$  and  $\mathbf{M}$  are considered parallel (equilibrium magnetization) (non-equilibrium magnetization leads to the existence of the magnetic torque and when the magnetization is not in equilibrium owing to time transients or time-varying magnetic fields, in order to fully describe the physics of the flow, a magnetization equation is necessary [48]), and the continuation of magnetic induction ( $\nabla \cdot \mathbf{B} = 0$ ) is assumed. Given the mentioned assumptions, according to reference [49], the continuity, momentum and energy equations governing the

flow are as follows, respectively:

$$\nabla \cdot V = 0 \quad (6)$$

$$\rho_{nf} (V \cdot \nabla) V = -\nabla P + \mu_{nf} \nabla^2 V - \rho_{nf} \beta_{nf} (T - T_0) g + \mu_0 M \nabla H + J \times B \quad (7)$$

$$(\rho c_p)_{nf} (V \cdot \nabla) T = k_{nf} \nabla^2 T + \mu_{nf} \Phi - \mu_0 T \frac{\partial M}{\partial T} (V \cdot \nabla) H + \frac{J \cdot J}{\sigma_{nf}} \quad (8)$$

where  $\Phi$  is the viscous dissipation function which is as follows:

$$\Phi = 2 \left[ \left( \frac{\partial u}{\partial x} \right)^2 + \left( \frac{\partial v}{\partial y} \right)^2 + \left( \frac{\partial w}{\partial z} \right)^2 \right] + \left( \frac{\partial v}{\partial x} + \frac{\partial u}{\partial y} \right)^2 + \left( \frac{\partial w}{\partial y} + \frac{\partial v}{\partial z} \right)^2 + \left( \frac{\partial u}{\partial z} + \frac{\partial w}{\partial x} \right)^2 - \frac{2}{3} \left( \frac{\partial u}{\partial x} + \frac{\partial v}{\partial y} + \frac{\partial w}{\partial z} \right)^2 \quad (9)$$

The magnetization is defined as [15]

$$M = M_s L(\xi) = \frac{6\phi m}{\pi d^3} \left( \coth(\xi) - \frac{1}{\xi} \right) \quad (10)$$

where  $\xi$  is the Langevin parameter and defined as

$$\xi = \frac{\mu_0 m H}{k_B T} \quad (11)$$

The volume of a unit cell of the crystal structure of magnetite is about  $730 \text{ \AA}^3$ . Each unit cell contains 8  $\text{Fe}_3\text{O}_4$  molecules, and each molecule has a magnetic moment of  $4 \mu_B$  [15]. Accordingly, the magnetic moment of the magnetite particles is calculated as [15]:

$$m = \frac{4\mu_B \pi d^3}{6 \times 91.25 \times 10^{-30}} \quad (12)$$

The magnetic field induction is defined as [50]

$$B = \mu_0 (H + M) \quad (13)$$

The terms  $\mu_0 M \nabla H$  and  $J \times B$  in Eq. (7) represent the magnetic force components per unit volume.  $\mu_0 M \nabla H$  is because of the magnetization and depends on the magnetic gradient.  $J \times B$  represents Lorentz force per unit volume because of the induced electric current. The terms  $\mu_0 T \partial M / \partial T (V \cdot \nabla) H$  and  $J \cdot J / \sigma_{nf}$  in Eq. (8) represent the thermal power per unit volume because of the magnetocaloric effect and Joule heating, respectively.

On the basis of the physical properties of the base fluid and nanoparticle, the properties of the nanofluid are defined as follow:

The density of the nanofluid is calculated as [51]

$$\rho_{nf} = (1 - \phi) \rho_f + \phi \rho_p \quad (14)$$

The viscosity of the nanofluid is approximated by the Brinkman model [51]

$$\mu_{nf} = \frac{\mu_f}{(1 - \phi)^{2.5}} \quad (15)$$

The heat capacitance of the nanofluid is defined as [51]

$$(\rho c_p)_{nf} = (1 - \phi) (\rho c_p)_f + \phi (\rho c_p)_p \quad (16)$$

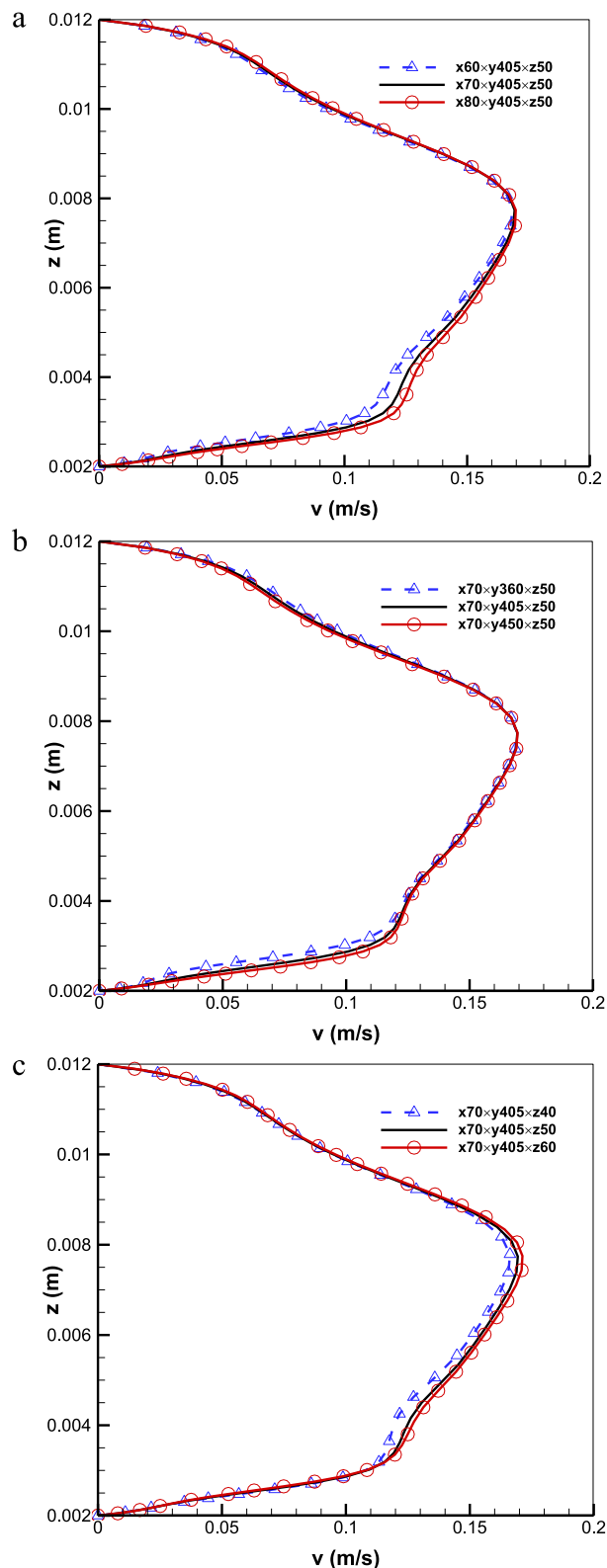
The thermal conductivity of the nanofluid is calculated by the Hamilton and Crosser model [52]

$$k_{nf} = \frac{k_p + (n - 1)k_f - (n - 1)\phi(k_f - k_p)}{k_p + (n - 1)k_f + \phi(k_f - k_p)} k_f \quad (17)$$

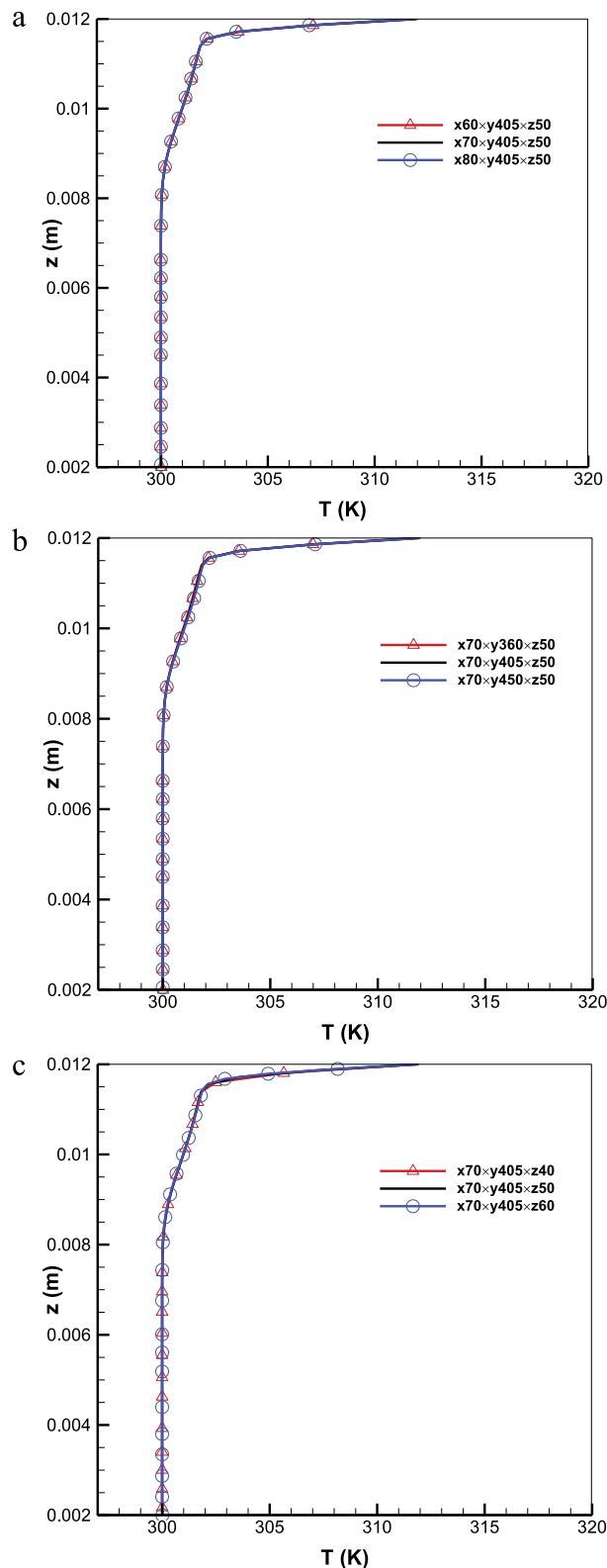
in which  $n$  is the empirical shape factor that is considered 3 for spherical particles.

The thermal expansion coefficient of the nanofluid is estimated as [51]

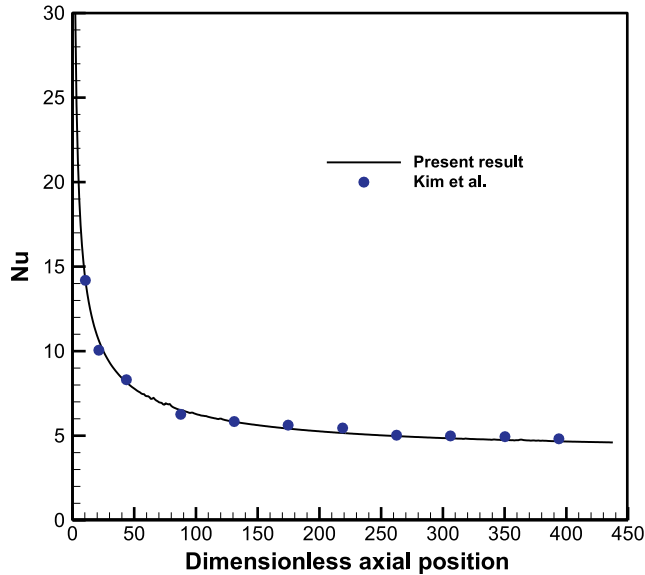
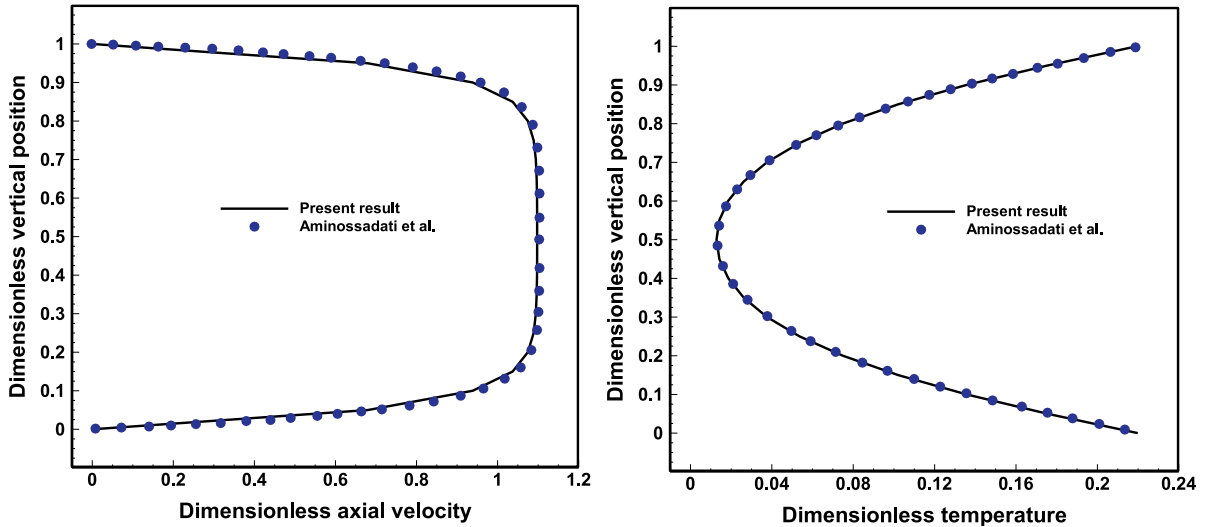
$$\beta_{nf} = \left( \frac{1}{1 + \frac{(1-\phi)\rho_f}{\phi\rho_p} \beta_f} + \frac{1}{1 + \frac{\phi\rho_p}{(1-\phi)\rho_f}} \right) \beta_f \quad (18)$$



**Fig. 2.** Axial velocity  $v$  for  $Re=850$ ,  $c=0.01$  m and  $D=0.002$  m on line at  $x=0$  and  $y=0.02$  m at different grid points along a)  $x$  direction, b)  $y$  direction, c)  $z$  direction.



**Fig. 3.** Temperature for  $Re=850$ ,  $c=0.01$  m and  $D=0.002$  m on line at  $x=0$  and  $y=0.02$  m at different grid points along a) x direction, b) y direction, c) z direction.

Fig. 4. Nusselt number in a horizontal tube where  $Re=1620$ .Fig. 5. Dimensionless velocity and temperature on the line of dimensionless axial position=50 at Hartmann number=20 in a channel where  $Re=100$ .

The electrical conductivity of the nanofluid using the model presented by Maxwell [53] is calculated as follows

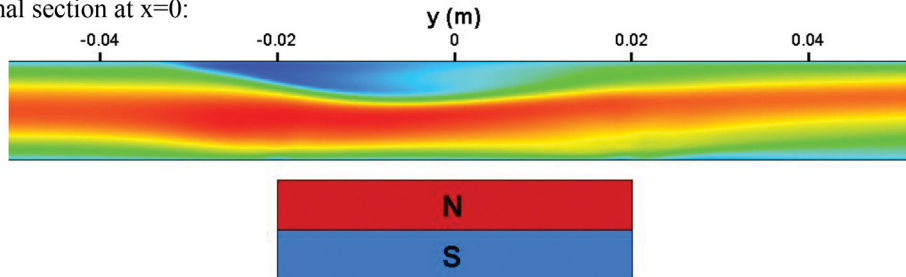
$$\sigma_{nf} = \left( 1 + \frac{3\left(\frac{\sigma_p}{\sigma_f} - 1\right)\phi}{\left(\frac{\sigma_p}{\sigma_f} + 2\right) - \left(\frac{\sigma_p}{\sigma_f} - 1\right)\phi} \right) \sigma_f \quad (19)$$

According to Eqs. (14) to (19) and Table 1, the properties of the water based ferrofluid with the nanoparticle volume fraction of 4% are  $\rho_{nf}=1166.3$ ,  $\mu_{nf}=0.0011108$ ,  $c_{pnf}=3555.6$ ,  $k_{nf}=0.6557$ ,  $\beta_{nf}=0.000175$  and  $\sigma_{nf}=0.05625$ .

## 2.2. Numerical method, grid independency and validation

In this study, ANSYS FLUENT via finite volume method was employed to numerically solve the governing equations while five User-Defined Functions (UDFs) were written and added to the software to apply the magnetic effects and fully developed velocity profile. For the velocity-pressure coupling and pressure correction equation, the PISO algorithm and PRESTO scheme were employed, respectively. Moreover, the Power law scheme was used to discretize the convective and diffusive terms.

longitudinal section at  $x=0$ :



cross sections:

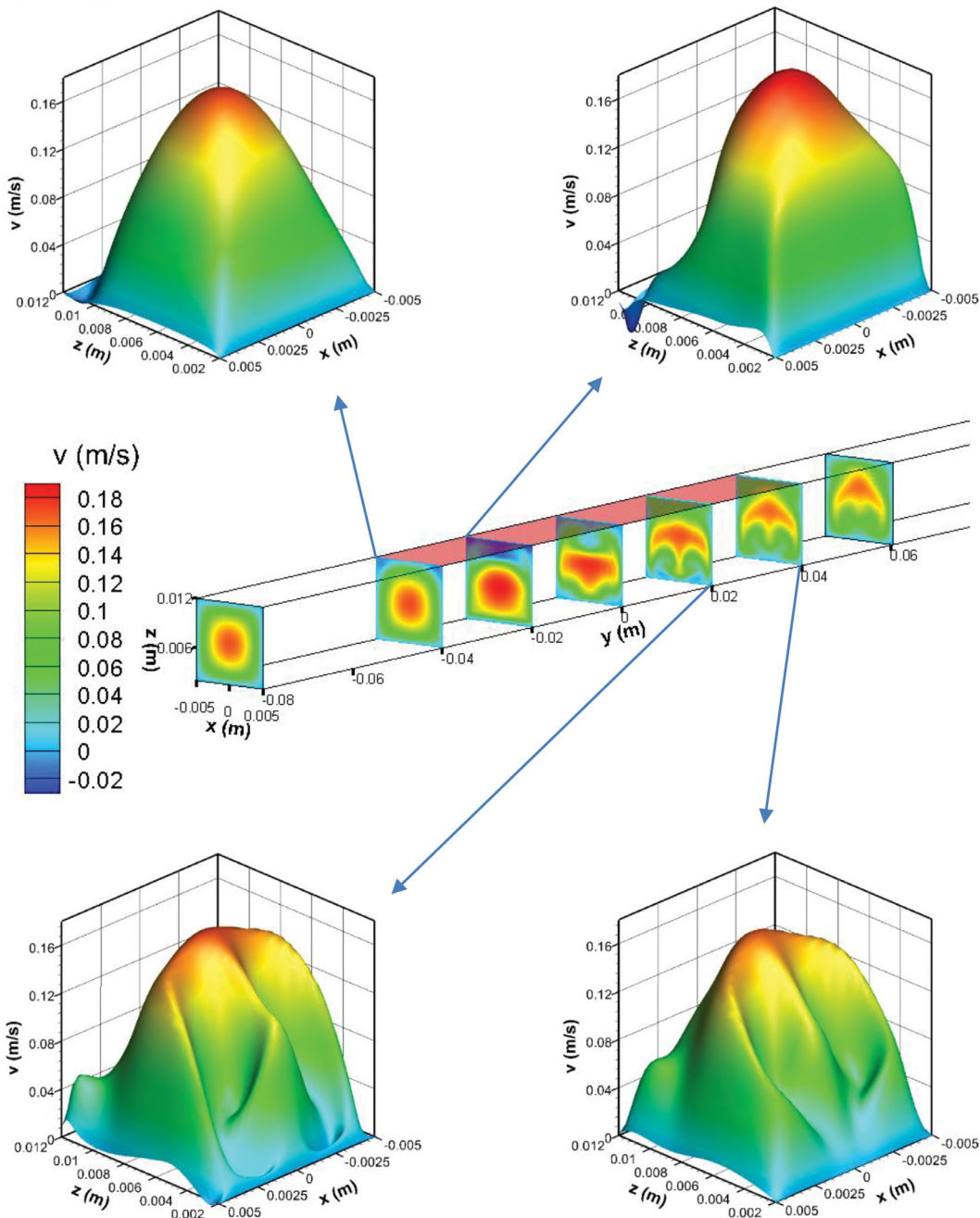


**Fig. 6.** Velocity contours for  $Re=850$ ,  $c=0.01$  m and  $D=0.002$  m.

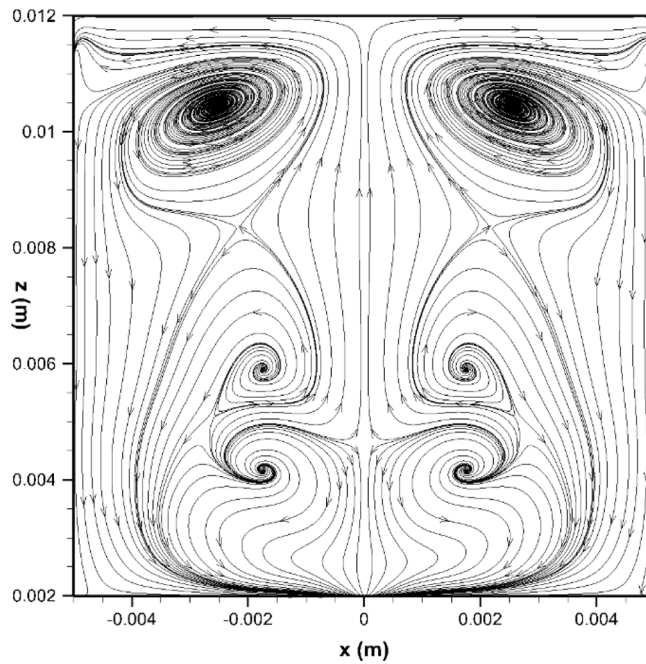


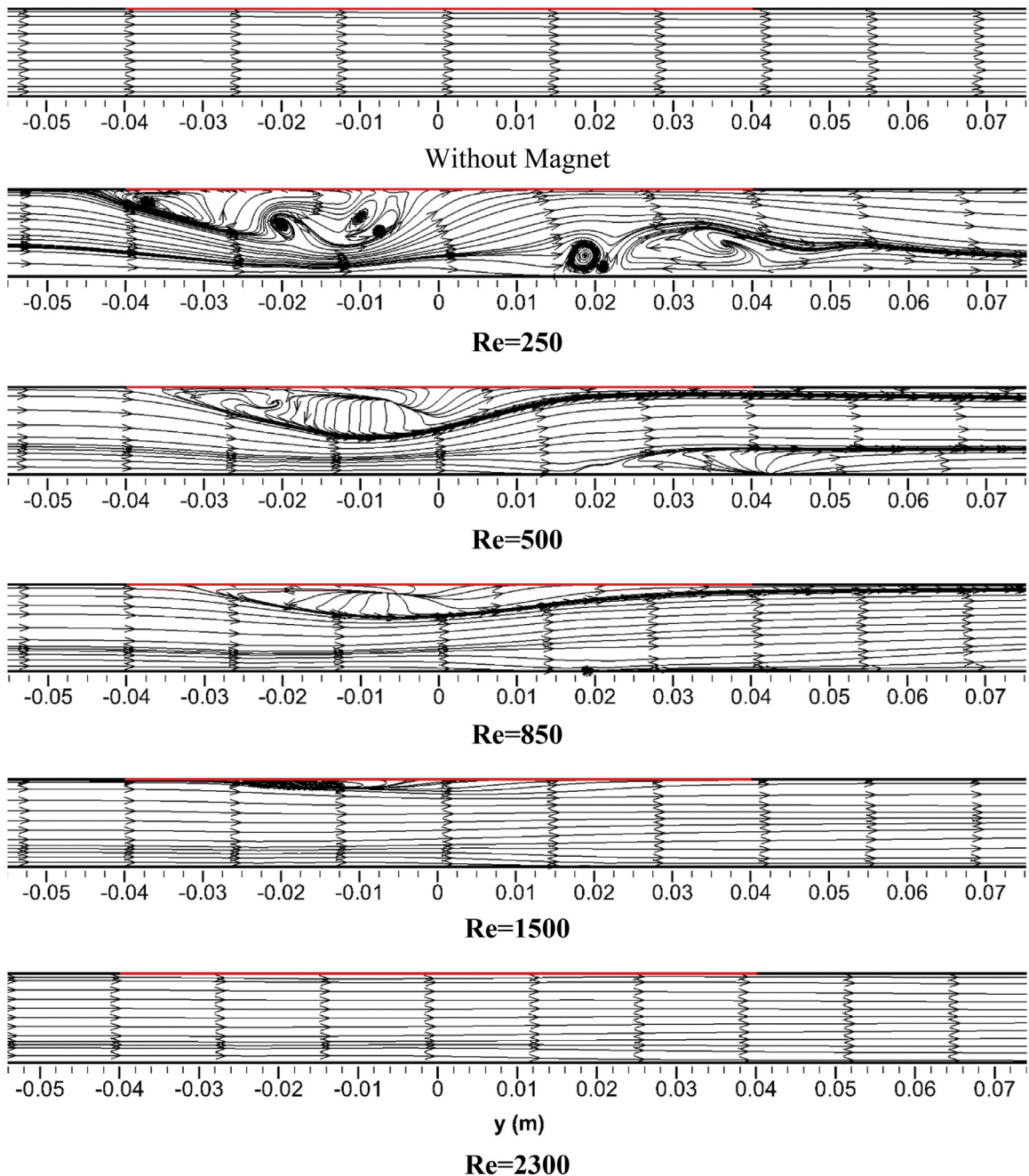
**Fig. 7.** Streamlines on cross section at  $y=0.02$  m for  $Re=850$ ,  $c=0.01$  m and  $D=0.002$  m.

The computational domain was discretized by a structured non-uniform grid. Considering that accurately covering the magnetic force by computational grids plays an essential role in the achievement of the results that are independent of the computational grid [54], some non-uniform grids were designed. Different non-uniform grid densities are examined to check the independency of the solution from the grid numbers. Along the x, y, and z directions, the grid independency is investigated by comparing the velocity and temperature profiles. The results shown in Fig. 2 and Fig. 3 reveal that the non-uniform grid with the size of  $70 \times 50 \times 405$  is appropriate for this simulation since by increasing the grid points in each direction, the results do not significantly change (Fig. 2 and Fig. 3). The temperature profiles (Fig. 3) are almost the same, but for the velocity, for example in Fig. 2(b), at the point  $z=0.003$  m, there is a difference of 10% between the axial velocities obtained from grids  $70 \times 360 \times 50$  and  $70 \times 405 \times 50$ . It might not be seen at first glance. The difference between the axial velocities obtained from grids  $70 \times 405 \times 50$  and  $70 \times 450 \times 50$  decreases to below 4% and therefore, it is concluded that computational grid  $70 \times 405 \times 50$  is appropriate.

The comparison of the present result with an experimental result [55] shown in Fig. 4 reveals that there is a reasonable agreement between the two results. Moreover, as shown in Fig. 5, in the presence of magnetic force, the comparison of the non-dimensional velocity and temperature profiles of the present solution with Aminossadati *et al.*'s results [56] reveals an excellent agreement between the results.

### 3. Results and discussion

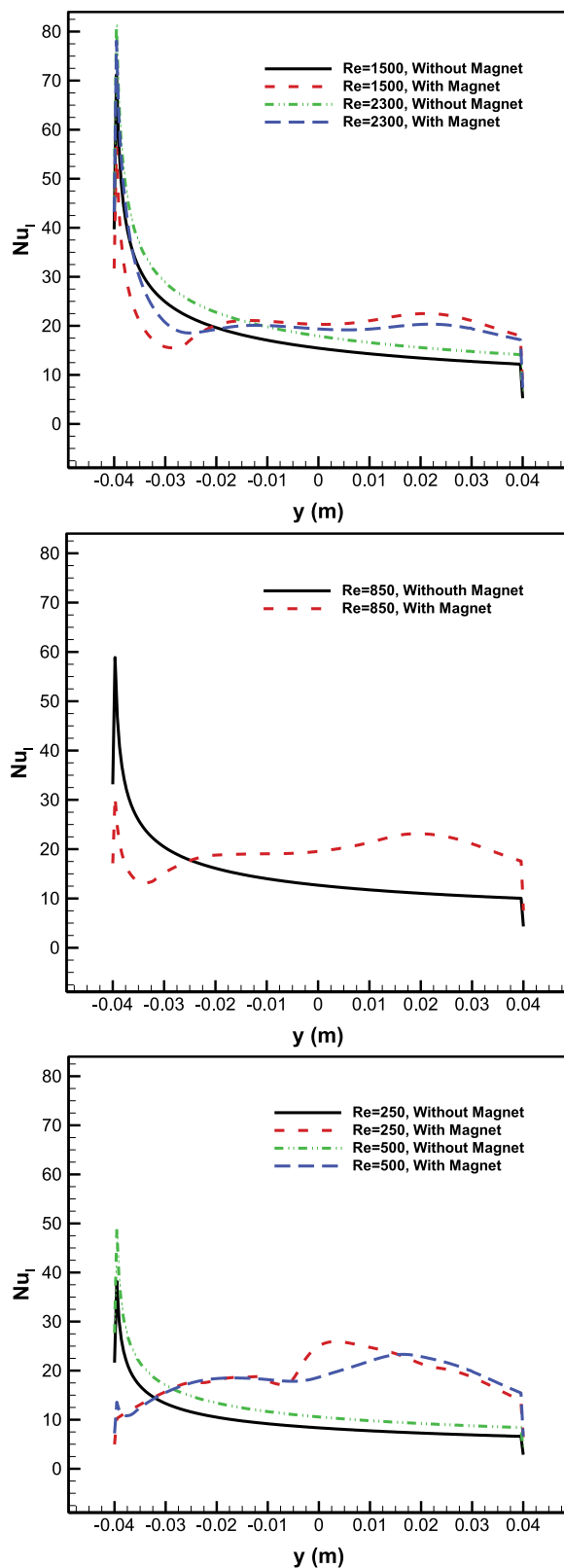
To investigate the effects of the magnetic field on the flow field, the velocity contours at the longitudinal and cross-sections of the channel are depicted in Fig. 6. The fully developed flow enters the channel and approaches the block magnet zone without any deviation in the velocity distribution where the flow is parallel. The hot surface is mounted at the top of the channel where the block magnet is located near the bottom of the channel. As it can be seen in the longitudinal section, the magnetic field of the permanent magnet diverts the flow and attracts the nanofluid. According to the momentum equations, the added source terms to the equations represent the magnetic forces and change the flow field. This phenomenon occurs a bit before the first edge of the block magnet ( $y=-0.03$ ). It reveals that the magnetic field is not limited to the region above of the block magnet and its influence exists in a larger region. The maximum velocity is at the center in the entrance and then moves lower in the magnetic zone. After that, an interesting phenomenon occurs. It is expected that the maximum velocity returns to the center of the channel as the nanofluid flows away from the magnetic field zone, but this does not occur, and the maximum velocity moves to the upper half of the channel. The velocity profiles shown at different sections along the channel indicate that after  $y=-0.04$ , the effect of the magnetic field becomes more significant. It seems that in this case, the velocity profile does not change further after  $y=0.04$  m. Further away from the magnet, the magnetic force weakens and cannot overcome the inertia force and therefore, is not able to significantly affect the flow field. Fig. 7 shows the streamlines on the cross-section at  $y=0.02$  m for  $Re=850$ ,  $c=0.01$  m and  $D=0.002$  m. It shows that applying the magnetic field causes the creation of secondary flow. The body forces applied by the magnetic field



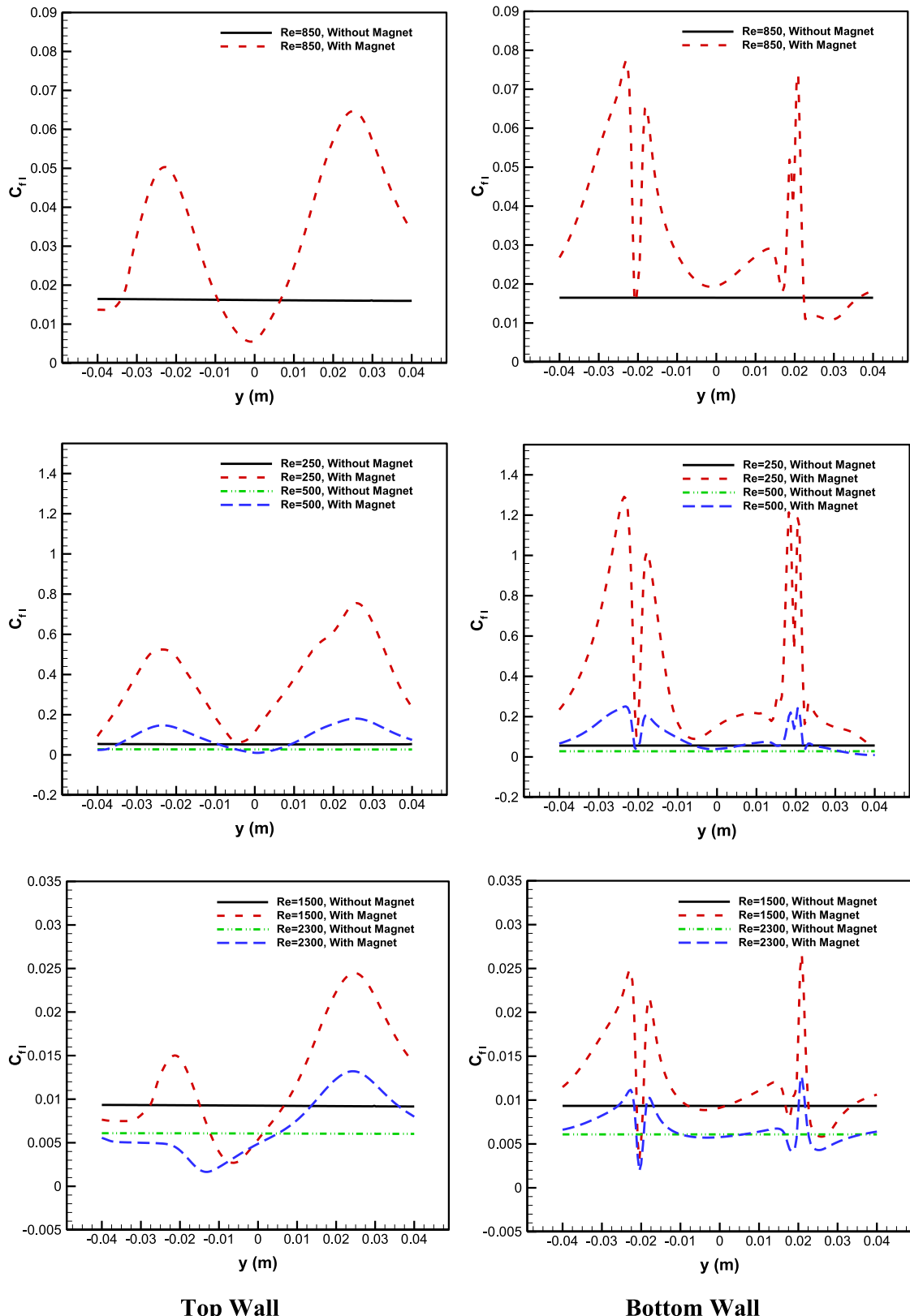
**Fig. 8.** Stream lines on longitudinal section at  $x=0$ ,  $c=0.01$  m and  $D=0.002$  m.

on the nanofluid flow are not in the same direction as the inertia force. In this situation, the streamlines are not merely parallel with the  $y$ -axis, and the nanofluid flows in the directions of  $x$  and  $z$  as the streamlines in the form of recirculation zones are seen in the  $x$ - $z$  cross-sectional plane (Fig. 7).

A comparison between the streamlines at different Reynolds numbers is performed in Fig. 8. Without the magnetic effect, the streamlines are parallel and horizontal. The hot surface is located at the top of the channel and therefore, natural convection does not exist. In this condition, forced convection and conduction are the dominant heat transfer mechanisms. At the low Reynolds number range, the forced convection is not strong, and in the absence of natural convection, the heat transfer is weak. In this configuration, creating mixed flow and disrupting the boundary layer near the hot surface might enhance the heat transfer. In the absence of the buoyancy force due to this particular configuration that is unavoidable in some applications, another body force like magnetic force could change the conditions. Fig. 8 shows that applying the



**Fig. 9.** Local Nusselt number,  $c=0.01$  m and  $D=0.002$  m.

**Fig. 10.** Local skin-friction coefficient,  $c=0.01$  m and  $D=0.002$  m.

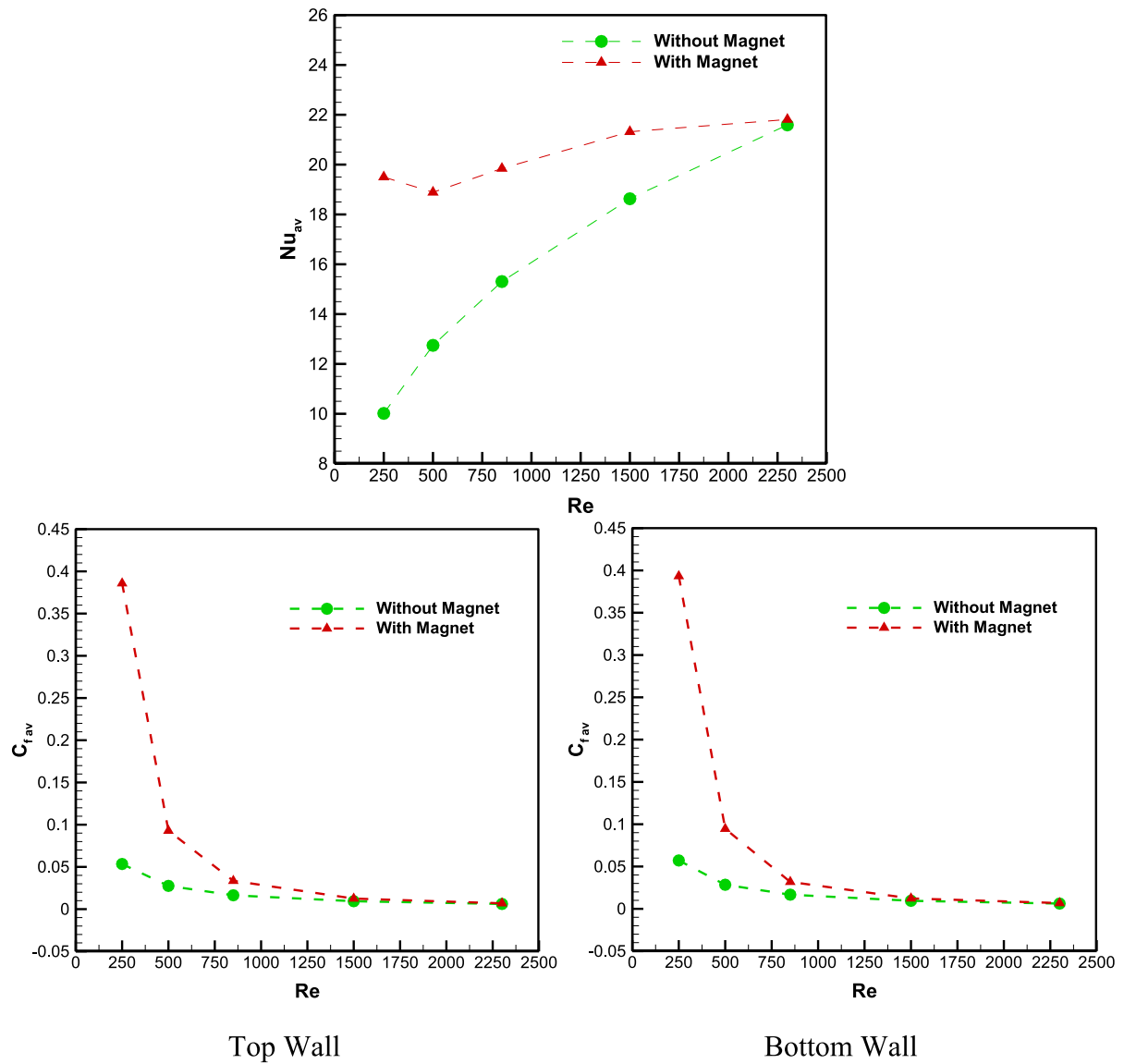
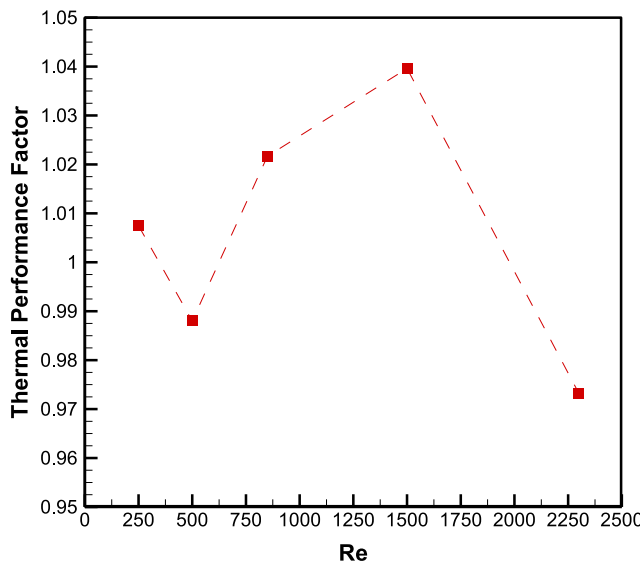


Fig. 11. Average Nusselt number and skin-friction coefficient,  $c=0.01$  m and  $D=0.002$  m.

magnetic force, originated from the block magnet, effectively disturbs the fluid flow causing the hot fluid moves downward, and a recirculation zone is formed at the top region of the channel near the hot surface. After the magnetic zone, the nanofluid moves upward again as the result of the first recirculation zone, and another recirculation zone is formed in the region close to the bottom of the channel. However, they disappear at the higher Reynolds numbers where in comparison with the inertia force, the magnetic force is not strong enough to divert the fluid flow.

The local Nusselt number along the hot top surface of the channel at different Reynolds numbers is plotted in Fig. 9. Without the magnetic effect, the Nusselt number at the first edge of the heated surface is high due to the large temperature gradient between the fluid flow and the hot surface. The Nusselt number gradually decreases along the hot wall as the thermal boundary layer becomes thicker and consequently, the temperature gradient decreases. Increasing the Reynolds number enhances the heat transfer without any changes in the plot trend. With the rise of the Reynolds number, the boundary layer becomes thinner and the heat transfer increases. In the presence of the block magnet, the trend of plots significantly changes where the local Nusselt number has different behavior at the various Reynolds numbers. For the high Reynolds numbers, where the inertia force is great enough, the maximum Nusselt number occurs at the first edge of the hot surface as identical as the cases without the magnetic effect. The reason given for this is that wherever the inertia force is dominant, the magnetic force is diminished. However, in the middle region of the hot surface where the fluid is close to the block magnet, and compared to other places the magnetic force is higher, the Nusselt number is higher than one for



**Fig. 12.** Thermal performance factor,  $c=0.01$  m and  $D=0.002$  m.

the case without the block magnet. At the low Reynolds numbers, the vortex near the hot surface induces a convection of the hot fluid at that region and decreases the temperature gradient at the initial edge and consequently, there are no very high values of the Nusselt number at the beginning of the hot top wall. By advancing on the hot surface, this convection induces a greater temperature gradient on the hot surface compared to the case without the magnetic field. Moreover, the recirculation zone that arises from the magnetic effect causes a quite uniform temperature gradient making the Nusselt plot somewhat flat. It can be concluded that the heat transfer is improved by applying the magnetic field in total. As the Reynolds number increases, the influence of the magnetic force on the flow decreases. In conclusion, it is found that the block magnet is more efficient at low Reynolds numbers.

Friction, as well as heat transfer, is important due to its direct impact on the pumping power and economic cost. Fig. 10 shows the variation of the friction factor along the hot top wall at different Reynolds numbers. It indicates that the friction factor has a little variation along the hot surface in the cases without the magnetic field, and it slightly decreases with the rise of the Reynolds number. In the presence of the block magnet, the formed vortices change the friction factor trend, especially at the low Reynolds number of 250. It is observed that the fluid flow before and after the region above the block magnet is also under the influence of the magnetic field. The friction factor grows up and reaches its first peak almost above the initial edge of the block magnet and then, it decreases. There are two peaks and one valley in the curve. The minimum friction factor occurs at the center of the permanent magnet while the peaks are almost above the edges of the block magnet related to the start and end of the recirculation zones. With the rise of Reynolds number, the differences between the cases with and without the block magnet are diminished. In addition, the friction factor on the bottom wall is studied in Fig. 10 (right column). Similar to the top wall, magnetic force changes and generally increases the friction factors.

The average Nusselt number versus different Reynolds numbers is shown in Fig. 11. It depicts that the magnetic field of the block magnet has a significant effect on the heat transfer at the low Reynolds number of 250, and the effect decreases with the rise of Reynolds number. In the presence of the block magnet below the channel, the heat transfer is enhanced by a factor of about 2 at  $Re=250$ . At the Reynolds of 250, the magnetic force greatly outweighs the inertia force and consequently, the flow is sharply drawn downwards leading to the formation of some vortices. These recirculation zones enhance the heat transfer significantly. With the rise of Reynolds number, the magnetic force in comparison to the inertia force becomes weaker and the vortices are diminished, and some vortices existing at  $Re=250$ , do not appear at higher Reynolds numbers. As mentioned before, the magnetic force induces a secondary flow near the hot surface and improves the heat transfer. As the Reynolds number increases from 500 to 2300, the Nusselt number increases about 70% and 15% for the cases without and with the block magnet, respectively. The variation of the Nusselt number versus Reynolds number for the case without the permanent magnet is greater than one for the case with the magnet. However, the Nusselt number for the case with the magnetic field is still greater than one for the case without the magnet. As mentioned before, the boundary layer becomes thinner with the rise of the Reynolds number of the flow over the flat plate and the heat transfer enhances. For the cases with the block magnet, the magnetic field creates a secondary flow and the boundary layer on the top surface is affected by this mixed flow. In this situation, the increase of Reynolds number does not enhance the heat transfer as well as it enhances for the case without the magnetic effect.

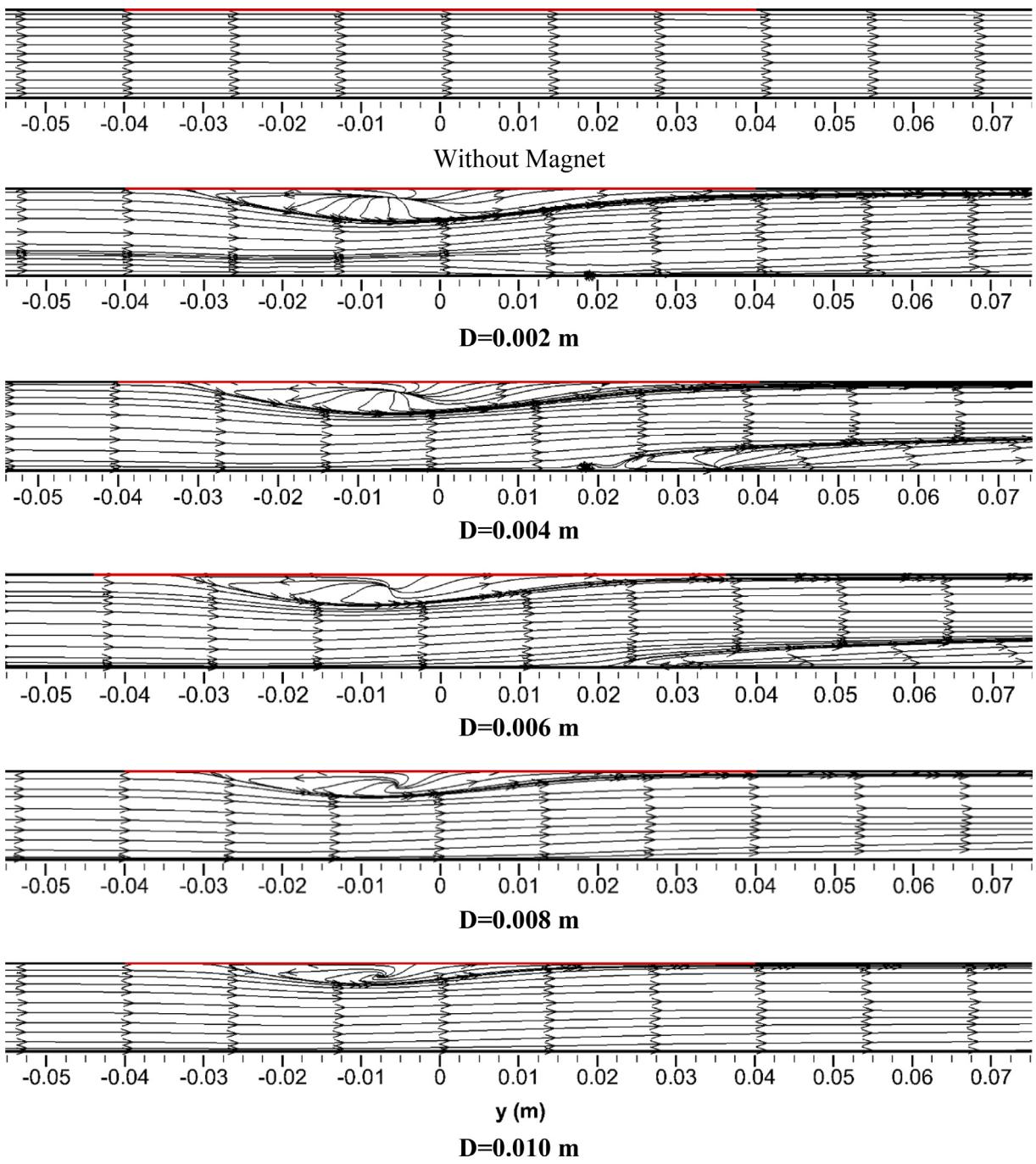


**Fig. 13.** Stream lines on longitudinal section at  $x=0$ ,  $c=0.01$  m and  $Re=850$ .

As shown in Fig. 11, in the absence of magnetic force, with the rise of Reynolds number, the friction factor decreases as the thickness of boundary layer reduces. Applying the magnetic field drastically increases the friction factor at the low Reynolds number of 250, where the friction factor increases by a factor of 8. It is due to the secondary flow close to the top wall, induced by the magnetic force. This might place severe limitations on the use of the block magnet due to the rise of pumping power. By diminishing the recirculation zones with the rise of the Reynolds number, the friction factor is sharply decreased where the difference of average friction factors for the cases with and without the block magnet becomes about 300% at the Reynolds number of 500.

The performance factors are defined to compare the proposed design with the reference design. There are three basic performance factors defined 1- to achieve the minimum heat transfer surface area ratio for identical pumping power and

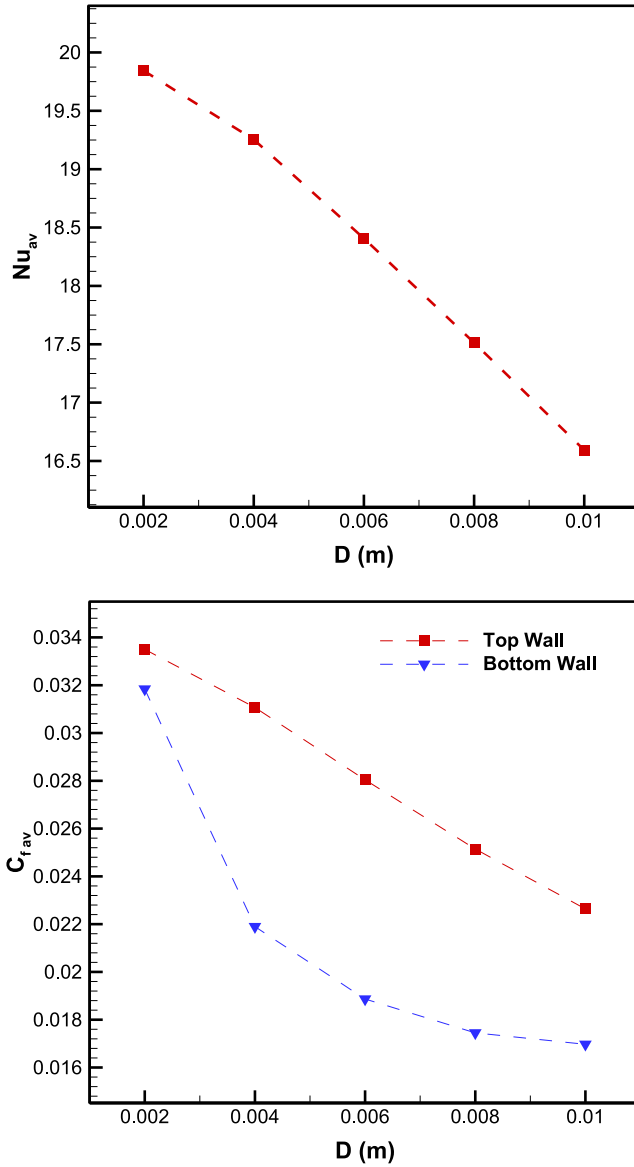


Fig. 14. Average Nusselt number and skin-friction coefficient,  $c=0.01$  m and  $Re=850$ .

heat duty, 2- to achieve the minimum pumping power for identical heat transfer surface area and heat duty and 3- to achieve the maximum heat duty for identical pumping power and heat transfer surface area [57]. In the present study, where the heat transfer area does not change, to evaluate the heat transfer enhancement at the identical pumping power, the thermal performance factor is calculated by Eq. (20) and plotted in Fig. 12. The figure shows that by applying the magnetic field, the thermal performance does not significantly change. In the presence of the magnetic field, the Reynolds number of 1500 has the maximum performance (1.04).

$$\text{ThermalPerformanceFactor} = \frac{\frac{Nu_{\text{withmagnet}}}{Nu_{\text{withoutmagnet}}}}{\left(\frac{C_f_{\text{withmagnet}}}{C_f_{\text{withoutmagnet}}}\right)^{\frac{1}{3}}} \quad (20)$$

The magnetic effect on the fluid flow decreases with the distance to the magnet as the magnetic source. The streamlines of the nanofluid for different distances between the magnet and channel are shown in Fig. 13. It can be seen that by increasing the distance, the recirculation zone near the top wall shrinks. The average Nusselt number decreases 16% with rise of the distance from 2 mm to 10 mm (Fig. 14). It reveals that the distance is an important parameter in the impact of the magnetic field on the heat transfer, and it should be as small as possible. In addition, the friction factor decreases with

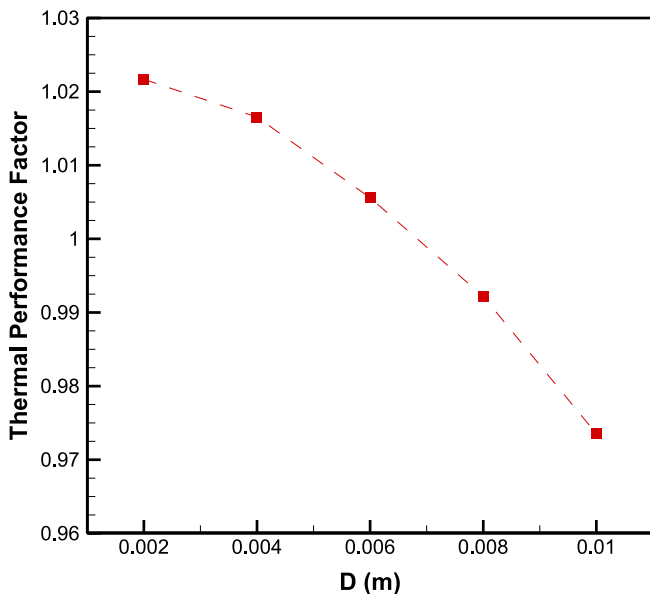


Fig. 15. Thermal performance factor,  $c=0.01$  m and  $Re=850$ .

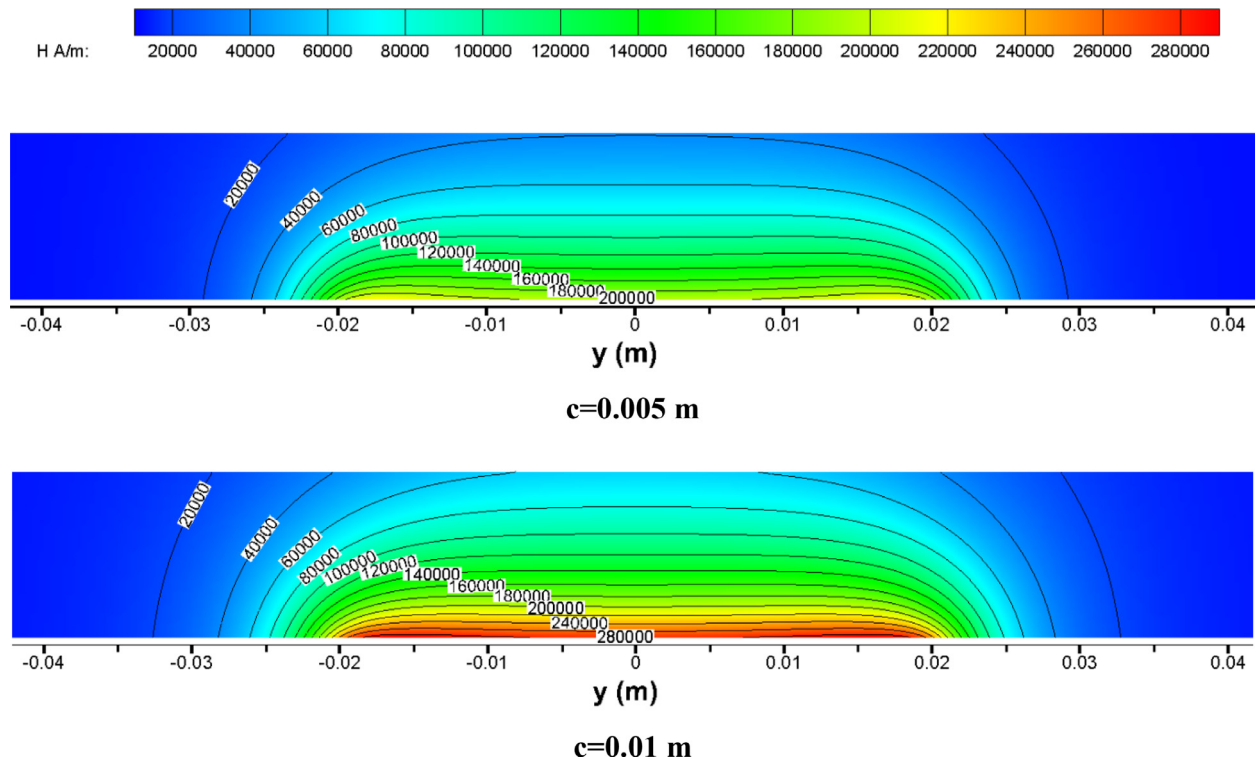
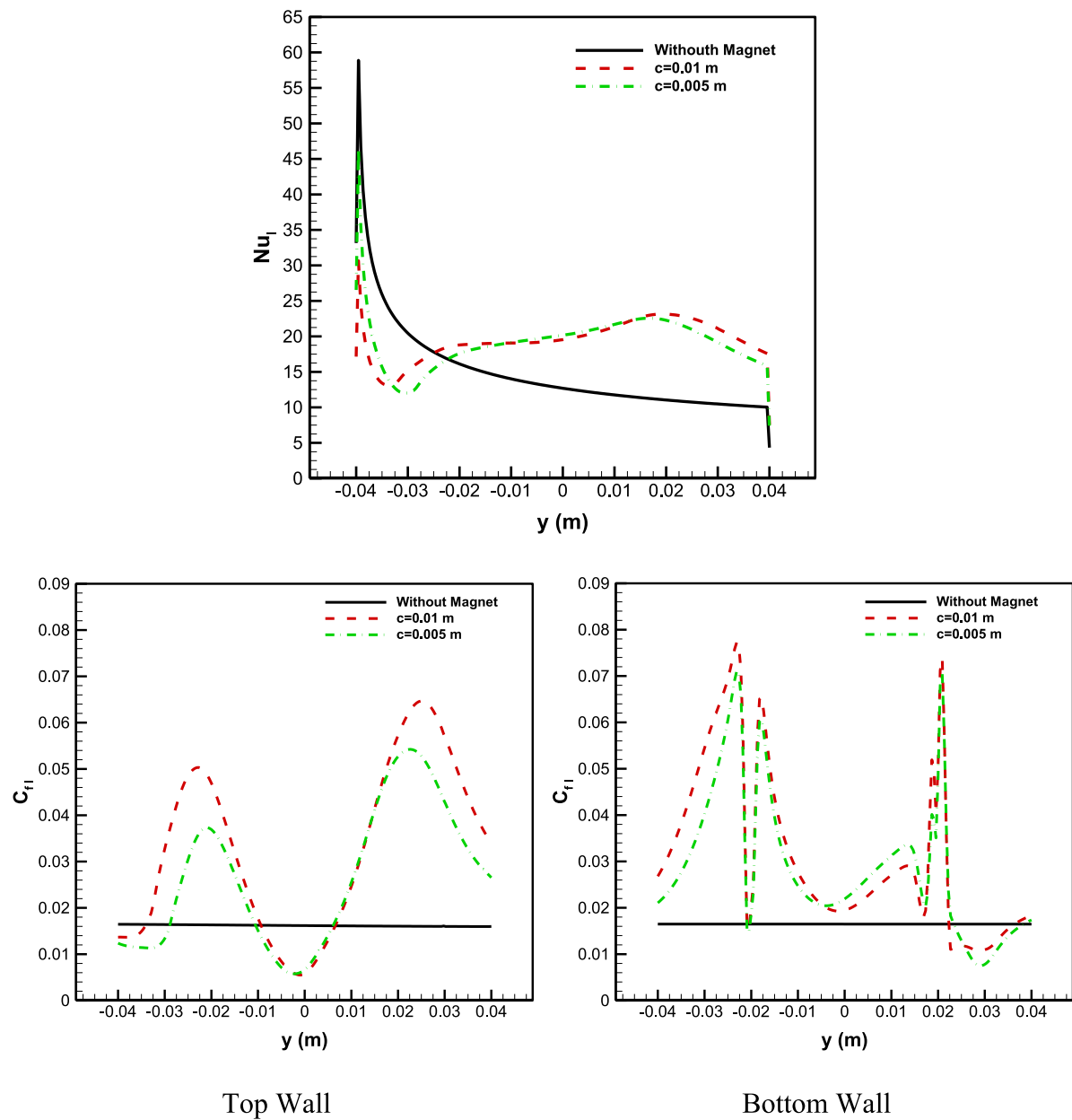


Fig. 16. Magnetic field intensity at  $x=0$ ,  $D=0.002$  m.

the distance, where for the top wall, it is reduced 32% by the increment of the distance from 2 mm to 10 mm. The thermal performance factor plot (Fig. 15) indicates that the factor decreases with increasing distance so that for the distances greater than 6 mm, the thermal performance becomes less than unity, which is not desirable.

The distribution of magnetic field intensity in the channel at  $x=0$  for two magnet thicknesses is shown in Fig. 16. It is clear that by decreasing the thickness, the strength of the magnet decreases. The effect of the variation of the block magnet height ( $c$ ) on the Nusselt number and friction factor is depicted in Fig. 17. It is indicated that by increasing the thickness,



**Fig. 17.** Local Nusselt number and skin-friction coefficient,  $D=0.002$  m and  $Re=850$ .

the Nusselt number changes only approximately before and after the magnet edges. As the magnet thickness decreases, the skin-friction coefficient over the top wall decreases more compared to the coefficient on the bottom wall. Moreover, considering the average Nusselt number and friction factor given in Table 2, as the height  $c$  decreases by half (from 1 cm to 0.5 cm), the thermal performance factor (Eq. (20)) increases 6% and becomes 1.086.

In order to investigate the separate effects arising from ferrohydrodynamics and magnetohydrodynamics on the fluid dynamics and heat transfer, the average body forces in the three directions and thermal powers that arise from FHD and MHD principles are extracted in different Reynolds numbers and shown in Table 3. The results reveal that the FHD effects are completely dominant, and the MHD effects are negligible. In the last row of Table 2, it can be seen that by omitting the MHD effects, the results do not change considerably. This means that the effects caused by the magnetization, which depend on the existence of magnetic gradient, are much stronger than the effects caused by the induced electric current.

**Table 2**Average Nusselt number and skin-friction coefficient,  $D=0.002$  m and  $Re=850$ .

	$Nu_{av}$	Top Wall $C_f_{av}$	Bottom Wall $C_f_{av}$
<b>Without Magnet</b>	15.306465	0.016395144	0.016713569
<b>c=0.005 m</b>	19.569826	0.027083816	0.029329658
<b>c=0.01 m</b>	19.844308	0.033500858	0.031840524
<b>c=0.01 m, Only FHD</b>	19.844306	0.033500854	0.03184053

**Table 3**

Average magnitude of magnetic components in whole computational domain.

		FHD	MHD
<b>x Magnetic Force Component per Unit Volume (N/m<sup>3</sup>)</b>	Re=250	12145.768	1.6e-06
	Re=500	12148.935	1.9e-06
	Re=850	12152.288	2.2e-06
	Re=1500	12154.921	2.7e-06
	Re=2300	12155.87	3.7e-06
<b>y Magnetic Force Component per Unit Volume (N/m<sup>3</sup>)</b>	Re=250	13068.418	9.2e-06
	Re=500	13076.522	1.60e-05
	Re=850	13082.589	2.26e-05
	Re=1500	13087.165	3.58e-05
	Re=2300	13089.698	5.35e-05
<b>z Magnetic Force Component per Unit Volume (N/m<sup>3</sup>)</b>	Re=250	64410.053	2.5e-06
	Re=500	64423.512	3.4e-06
	Re=850	64436.6	4.9e-06
	Re=1500	64447.233	7.9e-06
	Re=2300	64451.883	1.18e-05
<b>Magnetic Thermal Power per Unit Volume (W/m<sup>3</sup>)</b>	Re=250	168.12317	6e-07
	Re=500	244.19542	1.5e-06
	Re=850	357.60125	2.7e-06
	Re=1500	581.04736	6.8e-06
	Re=2300	868.25414	1.53e-05

#### 4. Conclusion

In the present work, to improve the heat transfer from the hot top wall, a block neodymium magnet with real features is considered under a channel in which water- $Fe_3O_4$  magnetic nanofluid flows. The effects of the magnet thickness and distance of the magnet from the channel on the Nusselt number, friction factor and thermal performance are numerically investigated. The main conclusions from this study are as follows:

- Using the permanent magnet creates a secondary flow that assists the convection heat transfer and enhances the heat transfer.
- Applying the magnetic field is more efficient in low Reynolds numbers where the heat transfer from the hot top surface in the absence of the natural convection is low.
- With the rise of Reynold number, the magnetic force becomes weaker than the inertia force, and the secondary flow shrinks.
- The Nusselt number increases by a factor of 2 in the presence of the block magnet at the low Reynolds number of 250.
- The maximum thermal performance occurs at the particular Reynolds number of 1500. The decrease of the magnet height from 1 cm to 0.5 cm and the distance between the magnet and channel improves the thermal performance.
- A comparison made between the FHD and MHD effects on the fluid dynamic and heat transfer reveals that the magnetization effects are far more influential than the induced electric current effects.

#### Acknowledgments

This work was supported by Iran National Science Foundation (INSF) [grant number 98020084].

#### References

- [1] S.U. Choi, J.A. Eastman, Enhancing thermal conductivity of fluids with nanoparticles, Argonne National Lab., IL (United States), 1995.
- [2] A. Rosa, R. Gontijo, F. Cunha, Laminar pipe flow with drag reduction induced by a magnetic field gradient, Applied Mathematical Modelling 40 (2016) 3907–3918.
- [3] S.M. Mousavi, M. Farhadi, K. Sedighi, A computational study of biomagnetic fluid flow in a channel in the presence of obstacles under the influence of the magnetic field generated by a wire carrying electric current, European Journal of Computational Mechanics 27 (2018) 302–321.
- [4] S.M. Mousavi, A.A.R. Darzi, O. ali Akbari, D. Toghraie, A. Marzban, Numerical study of biomagnetic fluid flow in a duct with a constriction affected by a magnetic field, Journal of Magnetism and Magnetic Materials 473 (2019) 42–50.
- [5] J. Jawdat, S. Momani, I. Hashim, Inhibition or enhancement of chaotic convection via inclined magnetic field, Applied Mathematical Modelling 38 (2014) 2996–3002.

- [6] S.M. Mousavi, M. Biglarian, A.A.R. Darzi, M. Farhadi, H.H. Afrouzi, D. Toghraie, Heat transfer enhancement of ferrofluid flow within a wavy channel by applying a non-uniform magnetic field, *Journal of Thermal Analysis and Calorimetry* 139 (2020) 3331–3343.
- [7] M.A. Bijarchi, M.B. Shafii, Experimental investigation on the dynamics of on-demand ferrofluid drop formation under a pulse-width-modulated nonuniform magnetic field, *Langmuir* 36 (2020) 7724–7740.
- [8] M.A. Bijarchi, A. Favaeh, S. Alborzi, M.B. Shafii, Experimental investigation of on-demand ferrofluid droplet generation in microfluidics using a Pulse-Width Modulation magnetic field with proposed correlation, *Sensors and Actuators B: Chemical* 329 (2021) 129274.
- [9] R.E. Rosensweig, *Ferrohydrodynamics*, Cambridge University Press, Cambridge, 1985.
- [10] J.A. Shercliff, *Textbook of magnetohydrodynamics*, (1965).
- [11] E.L. Sinatra, *Understanding the Interaction Between Blood Flow and an Applied Magnetic Field*, University of South Florida, 2010.
- [12] H. Yamaguchi, *Engineering fluid mechanics*, Springer, 2008.
- [13] R. Ganguly, S. Sen, I.K. Puri, Thermomagnetic convection in a square enclosure using a line dipole, *Physics of Fluids* 16 (2004) 2228–2236.
- [14] Q. Li, Y. Xuan, Experimental investigation on heat transfer characteristics of magnetic fluid flow around a fine wire under the influence of an external magnetic field, *Experimental Thermal and Fluid Science* 33 (2009) 591–596.
- [15] H. Aminfar, M. Mohammadpourfard, Y.N. Kahnoumoui, A 3D numerical simulation of mixed convection of a magnetic nanofluid in the presence of non-uniform magnetic field in a vertical tube using two phase mixture model, *Journal of magnetism and magnetic materials* 323 (2011) 1963–1972.
- [16] H. Aminfar, M. Mohammadpourfard, Y.N. Kahnoumoui, Numerical study of magnetic field effects on the mixed convection of a magnetic nanofluid in a curved tube, *International Journal of Mechanical Sciences* 78 (2014) 81–90.
- [17] L. Wang, Y. Wang, X. Yan, X. Wang, B. Feng, Investigation on viscosity of  $\text{Fe}_3\text{O}_4$  nanofluid under magnetic field, *International Communications in Heat and Mass Transfer* 72 (2016) 23–28.
- [18] S. Mousavi, N. Jamshidi, A. Rabienataj-Darzi, Numerical investigation of the magnetic field effect on the heat transfer and fluid flow of ferrofluid inside helical tube, *Journal of Thermal Analysis and Calorimetry* 137 (2019) 1591–1601.
- [19] Y. Cheng, D. Li, Experimental investigation on convection heat transfer characteristics of ferrofluid in a horizontal channel under a non-uniform magnetic field, *Applied Thermal Engineering* 163 (2019) 114306.
- [20] R. Azizian, E. Doroodchi, T. McKrell, J. Buongiorno, L. Hu, B. Moghtaderi, Effect of magnetic field on laminar convective heat transfer of magnetite nanofluids, *International Journal of Heat and Mass Transfer* 68 (2014) 94–109.
- [21] J. Wang, G. Li, H. Zhu, J. Luo, B. Sundén, Experimental investigation on convective heat transfer of ferrofluids inside a pipe under various magnet orientations, *International Journal of Heat and Mass Transfer* 132 (2019) 407–419.
- [22] M. Valitabar, M. Rahimi, N. Azimi, Experimental investigation on forced convection heat transfer of ferrofluid between two-parallel plates, *Heat and Mass Transfer* 56 (2020) 53–64.
- [23] A.P. Tetuko, S. Simbolon, T.G. Sitorus, R. Zurcher, R.K. Hadi, E.A. Setiadi, C. Kurniawan, M. Ginting, P. Sebayang, The effect of magnetic nano-fluids ( $\text{Fe}_3\text{O}_4$ ) on the heat transfer enhancement in a pipe with laminar flow, *Heat and Mass Transfer* 56 (2020) 65–74.
- [24] B. Sun, Y. Guo, D. Yang, H. Li, The effect of constant magnetic field on convective heat transfer of  $\text{Fe}_3\text{O}_4/\text{water}$  magnetic nanofluid in horizontal circular tubes, *Applied Thermal Engineering* 171 (2020) 114920.
- [25] G. WEIR, G. CHISHOLM, J. LEVENEUR, THE MAGNETIC FIELD ABOUT A THREE-DIMENSIONAL BLOCK NEODYMIUM MAGNET, *The ANZIAM Journal* (2021) 1–20.
- [26] P. Naphon, S. Wiriyasart, Experimental study on laminar pulsating flow and heat transfer of nanofluids in micro-fins tube with magnetic fields, *International Journal of Heat and Mass Transfer* 118 (2018) 297–303.
- [27] J.-H. Seo, M.-Y. Lee, Illuminance and heat transfer characteristics of high power LED cooling system with heat sink filled with ferrofluid, *Applied Thermal Engineering* 143 (2018) 438–449.
- [28] C. Qi, J. Tang, F. Fan, Y. Yan, Effects of magnetic field on thermo-hydraulic behaviors of magnetic nanofluids in CPU cooling system, *Applied Thermal Engineering* 179 (2020) 115717.
- [29] F. Fan, C. Qi, J. Tang, Q. Liu, X. Wang, Y. Yan, A novel thermal efficiency analysis on the thermo-hydraulic performance of nanofluids in an improved heat exchange system under adjustable magnetic field, *Applied Thermal Engineering* 179 (2020) 115688.
- [30] S.M. Mousavi, B. Ehteshami, A.A.R. Darzi, Two-and-three-dimensional analysis of Joule and viscous heating effects on MHD nanofluid forced convection in microchannels, *Thermal Science and Engineering Progress* 25 (2021) 100983.
- [31] S. Miltenyi, W. Müller, W. Weichel, A. Radbruch, High gradient magnetic cell separation with MACS, *Cytometry* 11 (1990) 231–238.
- [32] Y. Haik, V. Pai, C.-J. Chen, Development of magnetic device for cell separation, *Journal of magnetism and magnetic materials* 194 (1999) 254–261.
- [33] M. Hejazian, W. Li, N.-T. Nguyen, Lab on a chip for continuous-flow magnetic cell separation, *Lab on a Chip* 15 (2015) 959–970.
- [34] O. Oduwole, S. Sheard, Three-dimensional mathematical modelling of magnetic bead interactions within a magnetic separation system, *Applied Mathematical Modelling* 45 (2017) 123–133.
- [35] B.B. Yellen, Z.G. Forbes, D.S. Halverson, G. Fridman, K.A. Barbee, M. Chorny, R. Levy, G. Friedman, Targeted drug delivery to magnetic implants for therapeutic applications, *Journal of magnetism and magnetic materials* 293 (2005) 647–654.
- [36] P. Cregg, K. Murphy, A. Mardinoglu, Inclusion of interactions in mathematical modelling of implant assisted magnetic drug targeting, *Applied Mathematical Modelling* 36 (2012) 1–34.
- [37] X. Zhang, M. Luo, E. Wang, L. Zheng, C. Shu, Numerical simulation of magnetic nano drug targeting to atherosclerosis: Effect of plaque morphology (stenosis degree and shoulder length), *Computer Methods and Programs in Biomedicine* 195 (2020) 105556.
- [38] M. Liangruksa, R. Ganguly, I.K. Puri, Parametric investigation of heating due to magnetic fluid hyperthermia in a tumor with blood perfusion, *Journal of magnetism and magnetic materials* 323 (2011) 708–716.
- [39] B. Lahiri, S. Ranoo, J. Philip, Magnetic hyperthermia study in water based magnetic fluids containing TMAOH coated  $\text{Fe}_3\text{O}_4$  using infrared thermography, *Infrared Physics & Technology* 80 (2017) 71–82.
- [40] K.-C. Liu, T.-M. Chen, Analysis of the thermal response and requirement for power dissipation in magnetic hyperthermia with the effect of blood temperature, *International Journal of Heat and Mass Transfer* 126 (2018) 1048–1056.
- [41] Y.-d. Tang, T. Jin, R.C. Flesch, Effect of mass transfer and diffusion of nanofluid on the thermal ablation of malignant cells during magnetic hyperthermia, *Applied Mathematical Modelling* 83 (2020) 122–135.
- [42] T.Z. Nursal, N. Bal, R. Anarat, T. Colakoglu, T. Noyan, G. Moray, M. Haberal, Effects of a static magnetic field on wound healing: results in experimental rat colon anastomoses, *The American journal of surgery* 192 (2006) 76–81.
- [43] S.L. Henry, M.J. Concannon, G.J. Yee, The effect of magnetic fields on wound healing: experimental study and review of the literature, *Eplasty* 8 (2008).
- [44] M. MacCaig, Permanent magnets in theory and practice, Pentech press, 1987.
- [45] C.M. Oldenburg, S.E. Borglin, G.J. Moridis, Numerical simulation of ferrofluid flow for subsurface environmental engineering applications, *Transport in Porous Media* 38 (2000) 319–344.
- [46] R.K. Shah, A.L. London, Chapter VII - Rectangular Ducts, in: R.K. Shah, A.L. London (Eds.), *Laminar Flow Forced Convection in Ducts*, Academic Press, 1978, pp. 196–222.
- [47] H. Aminfar, M. Mohammadpourfard, F. Mohseni, Two-phase mixture model simulation of the hydro-thermal behavior of an electrical conductive ferrofluid in the presence of magnetic fields, *Journal of magnetism and magnetic materials* 324 (2012) 830–842.
- [48] D.D. de Carvalho, R.G. Gontijo, Magnetization diffusion in duct flow: The magnetic entrance length and the interplay between hydrodynamic and magnetic timescales, *Physics of Fluids* 32 (2020) 072007.
- [49] E. Tzirtzikakis, A mathematical model for blood flow in magnetic field, *Physics of Fluids* 17 (2005) 077103.
- [50] R.E. Rosensweig, Heating magnetic fluid with alternating magnetic field, *Journal of magnetism and magnetic materials* 252 (2002) 370–374.

- [51] K. Khanafer, K. Vafai, M. Lightstone, Buoyancy-driven heat transfer enhancement in a two-dimensional enclosure utilizing nanofluids, *International Journal of Heat and Mass Transfer* 46 (2003) 3639–3653.
- [52] R. Hamilton, O. Crosser, Thermal conductivity of heterogeneous two-component systems, *Industrial & Engineering chemistry fundamentals* 1 (1962) 187–191.
- [53] A.H. Mahmoudi, I. Pop, M. Shahi, F. Talebi, MHD natural convection and entropy generation in a trapezoidal enclosure using Cu–water nanofluid, *Computers & Fluids* 72 (2013) 46–62.
- [54] S.M. Mousavi, M. Farhadi, K. Sedighi, Effect of non-uniform magnetic field on biomagnetic fluid flow in a 3D channel, *Applied Mathematical Modelling* 40 (2016) 7336–7348.
- [55] D. Kim, Y. Kwon, Y. Cho, C. Li, S. Cheong, Y. Hwang, J. Lee, D. Hong, S. Moon, Convective heat transfer characteristics of nanofluids under laminar and turbulent flow conditions, *Current Applied Physics* 9 (2009) e119–e123.
- [56] S. Aminossadati, A. Raisi, B. Ghasemi, Effects of magnetic field on nanofluid forced convection in a partially heated microchannel, *International Journal of Non-Linear Mechanics* 46 (2011) 1373–1382.
- [57] Y. Dong, L. Huixiong, C. Tingkuan, Pressure drop, heat transfer and performance of single-phase turbulent flow in spirally corrugated tubes, *Experimental Thermal and Fluid Science* 24 (2001) 131–138.